

PCCP

Accepted Manuscript



This article can be cited before page numbers have been issued, to do this please use: L. Veronese, E. Quartapelle Procopio, T. Moehl, M. Panigati, K. Nonomura and A. Hagfeldt, *Phys. Chem. Chem. Phys.*, 2019, DOI: 10.1039/C9CP00856J.



This is an Accepted Manuscript, which has been through the Royal Society of Chemistry peer review process and has been accepted for publication.

Accepted Manuscripts are published online shortly after acceptance, before technical editing, formatting and proof reading. Using this free service, authors can make their results available to the community, in citable form, before we publish the edited article. We will replace this Accepted Manuscript with the edited and formatted Advance Article as soon as it is available.

You can find more information about Accepted Manuscripts in the [author guidelines](#).

Please note that technical editing may introduce minor changes to the text and/or graphics, which may alter content. The journal's standard [Terms & Conditions](#) and the ethical guidelines, outlined in our [author and reviewer resource centre](#), still apply. In no event shall the Royal Society of Chemistry be held responsible for any errors or omissions in this Accepted Manuscript or any consequences arising from the use of any information it contains.

Triarylamine-based hydrido-carboxylate rhenium(I) complexes as photosensitizers for dye-sensitized solar cells.

Lorenzo Veronese,^{a,b} Elsa Quartapelle Procopio,^a Thomas Moehl,^c Monica Panigati,^{*,a,b} Kazuteru Nonomura,^{*,d} Anders Hagfeldt^d

^a Università degli Studi di Milano, Dipartimento di Chimica, Via Golgi 19, 20133 Milano (Italy)

^b Istituto per lo Studio delle Macromolecole, Consiglio Nazionale delle Ricerche (ISMAR-CNR), Via E. Bassini, 15, 20133 Milano, Italy

^c Department of Chemistry, University of Zurich, Winterthurerstrasse 190, CH-8057, Zürich (Switzerland)

^d Laboratory for Photomolecular Science, ISIC, École Polytechnique Fédérale de Lausanne, CH-1015 Lausanne (Switzerland)

Two new dyes based on dinuclear rhenium complex and (E)-3-(5-(4-(bis(2',4'-dibutoxy-[1,1'-biphenyl]-4-yl)amino)phenyl)thiophen-2-yl)-2-cyanoacrylic acid (namely **D35**) have been investigated as sensitizers for dye sensitized solar cells (DSSCs). Two different pyridazine ligands have been used, namely 4-pyridazine-carboxylic acid for dye **2** ($[\text{Re}_2(\mu\text{-H})(\text{-D35})(\text{CO})_6(\mu\text{-pyridazine-4-COOH})]$) and 4-pyridazinyl-butanoic acid for dye **3** ($[\text{Re}_2(\mu\text{-H})(\text{-D35})(\text{CO})_6(\mu\text{-pyridazine-4-C}_3\text{H}_6\text{-COOH})]$). The performances of these new dyes have been compared with those of the dye containing the bare 4-diphenylaminobenzoic acid, namely TPA, as ancillary ligand (dye **1**). Compared to dye **1**, dyes **2** and **3** show an impressive tenfold increase in the absorption intensity in the range 487–493 nm on TiO_2 films, with great improvement of the light harvesting. Cyclic voltammetry experiments, performed on the derivatives containing the methyl ester of the pyridazine ligands, show narrow electrochemical band gaps in the range of 1.36–1.84 eV. Solar cells with each dye have been prepared, using both iodide/triiodide and cobalt redox couples as electrolytes, platinum or carbon as counter electrodes, and TiO_2 or SnO_2 as metal oxide photoelectrodes respectively. The best DSSC results have been obtained using dye **3**, with an overall solar-to-electric conversion efficiency of 3.5%, which greatly overcomes the previous result of 1.0% obtained for dye **1** in a not-optimized setup of the device. The performances of dye **3** are due both to the presence of **D35** ligand, which further suppresses the recombination of the injected electron with the electrolyte and with the oxidized state of the dye.

Introduction

Dye Sensitized Solar Cells (DSSC)¹ are hybrid nanostructured organic/inorganic cells that have attracted huge attention so far from both academy and industry, due to the use of abundant, cheap materials and simple, low cost fabrication processes, that can be applied to both rigid (glass) and flexible (plastics, metals) substrates² and easily scaled up.³

In its simplest assembly, a DSSC is an electrochemical cell with two electrodes and an electrolyte filled in the space between them. The highest efficiency reported for small area DSSC based on ruthenium dye and iodide/triiodide electrolyte is 12.1%⁴ with long-term stability,⁵ while an efficiency as high as 13% was achieved using a molecularly engineered porphyrin dye in combination with a cobalt-based electrolyte.⁶

The most commonly used dyes in DSSC are complexes of ruthenium, containing organic ligands functionalized with carboxylic substituents as anchoring groups to the TiO_2 .⁷ These poly-pyridine complexes are characterized by intense and broad absorptions due to metal-to-ligand charge transfer (MLCT) transitions, longer excited states lifetime, and long-term chemical stability.⁸ Alternative dyes based on different metal complexes such as iron,⁹ copper¹⁰ and platinum¹¹ mainly containing bipyridine ligands, have been investigated so far,¹² while no example of rhenium complexes used as dye in operating solar cells has been reported in literature. In order to cover this gap and following some preliminary studies concerning the electron transfer from Re-polypyridyl complexes to nano-crystalline TiO_2 ¹³ we recently reported the first example of hydrido rhenium complexes employed in an operating DSSC.¹⁴ The best results have been obtained for the hydrido-carboxylato complex containing a triarylamine moiety (**1**, see Chart 1) which suppresses the recombination of the injected electron with the oxidized state of the complex, thus improving the charge separation on TiO_2 . Moreover, the bulky triarylamine moiety also reduces the back reaction of the injected electron with the electrolyte. Even if the maximum power conversion efficiency has been about 1%, these results have provided a sufficiently clear picture of the critical factors and of the lines to follow to improve the performances.

Therefore, in order to follow these lines, we report here on the design and the preparation, based on a novel and versatile three-step procedure, of two new hydrido-carboxylate dinuclear organometallic rhenium complexes, namely **2** and **3** (see Chart 1) endowed with the more conjugated TPA linker (E)-3-(5-(4-(bis(2',4'-dibutoxy-[1,1'-biphenyl]-4-yl)amino)phenyl)thiophen-2-yl)-2-cyanoacrylic acid a.k.a. DN-F04 dye (from now on, **D35**, see Chart 1). The interest in organic molecules, characterized by a D- π -A electronic structure, as dyes in DSSCs has been growing quickly the past decade, due to their non-limited feedstock, improved prerequisites for scalability, recycling issues and economy on a large scale. The absorption spectrum of **D35** makes it a reference organic dye for DSSCs. Excellent device stability has been obtained both under light and after at least 1000 h storage in darkness at temperatures of 85 °C^{15,16} and it is interesting also for indoor application due to a good match with fluorescent light and an attractive orange color. Therefore, we have linked **D35** as bridging ligand to the dinuclear rhenium complexes, to extend the light harvesting capacity and to allow their usage in cobalt-based electrolytes.

Looking at the anchoring group, one of the reason of the observed low efficiency of the previously reported complexes is the excessive stabilization of the π^* orbitals of the 4-carboxy-pyridazine, which partially hampers the electron injection into TiO_2 .¹⁴

In order to overcome this problem we report here a new dye (**3** in Chart 1) containing a diazine ligand endowed with an alkylic chain. Actually, the presence of electron-donor substituents in the β positions of the diazine ligand raises the LUMO level of the dye¹⁷ and then fosters the electron injection into the semiconductor.

These new dyes have been characterized from the spectroscopic and electrochemical point of view. Solar cells with each dye have been prepared and their performances have also been reported, using both iodide/triiodide and cobalt redox couples as electrolytes, platinum or carbon as counter electrodes, and TiO₂ (and partially SnO₂) as metal oxide photoelectrode. The performances have been compared to those obtained for **D35** and discussed in relation to the molecular structure of the dyes and to the previous results obtained for dye **1** in a not optimized setup of the device.

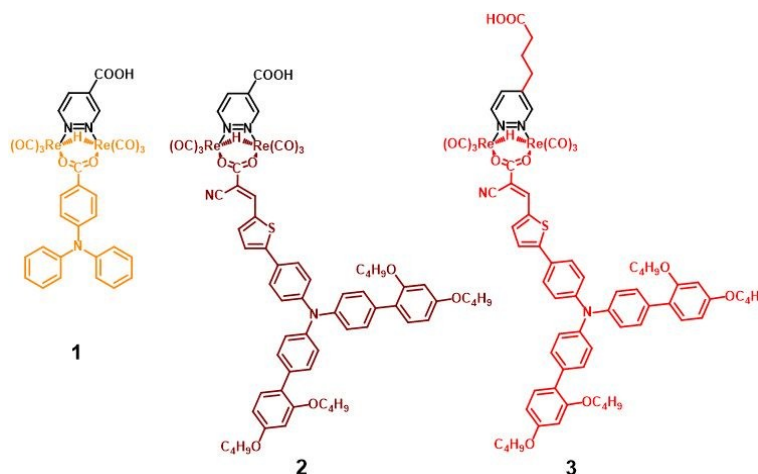


Chart 1: Molecular structure of the investigated dyes used as sensitizers

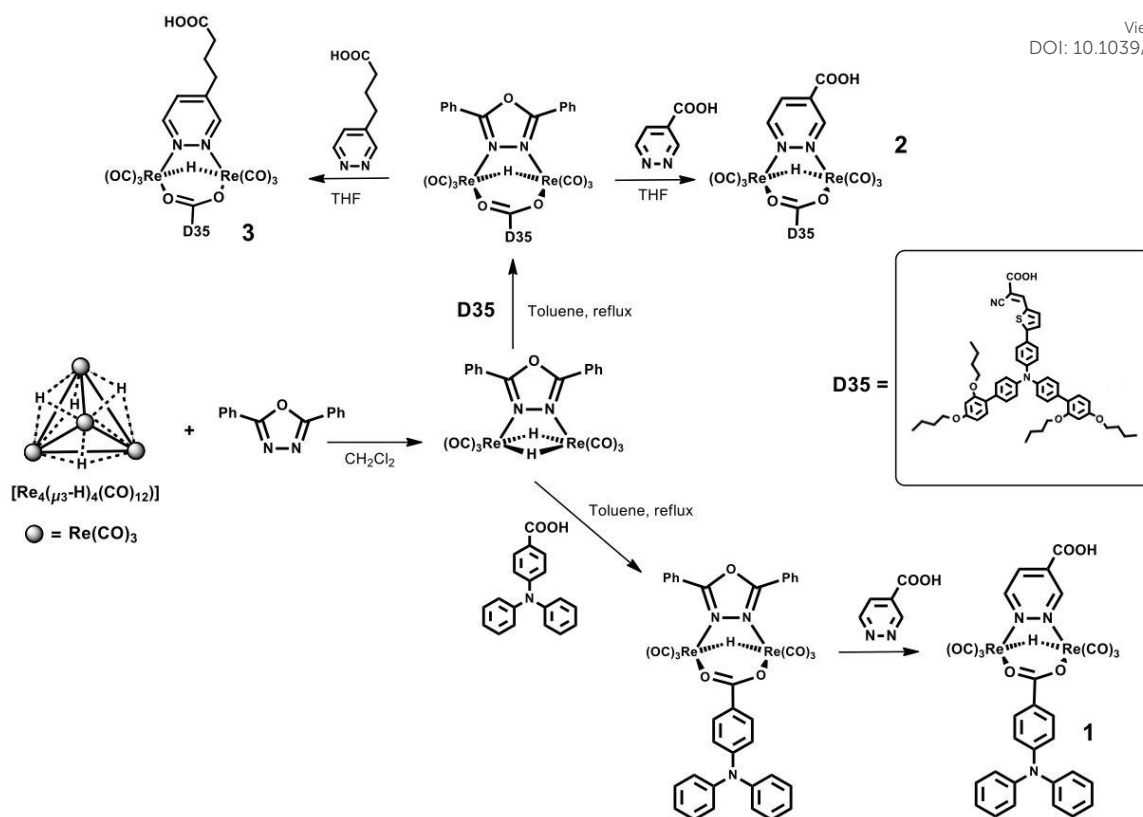
Results and discussion

Synthesis of the dyes

The hydrido-carboxylato derivatives **2** and **3** have been prepared exploiting the same three-step synthetic procedure already developed for the synthesis of the TPA-based derivative **1**.¹⁴ This procedure, shown in scheme 1, is based on the peculiar reactivity of the tetrahedral hydrido-carbonyl cluster [Re₄(μ_3 -H)₄(CO)₁₂] with bridging donor ligands as 2,5-diphenyl-1,3,4-oxadiazole (ppd), a sterically hindered heterocycle which contains two aromatic substituents in the α positions of the oxadiazole ring.¹⁸ In the first step the [Re₂(μ -H)₂(CO)₆(μ -ppd)] intermediate has been obtained in high yields by reacting [[Re₄(μ_3 -H)₄(CO)₁₂] with two equivalents of ppd at room temperature in CH₂Cl₂ solution.¹⁸ Then, the mixed hydrido-carboxylato complexes [Re₂(μ -H)(μ -OOCR)(CO)₆(μ -ppd)] (Scheme 1) have been obtained by reaction 1, which exploits the reactivity of the hydride ligands towards the acidic proton of any carboxylic acid. Through a simple acid-base reaction one of the two hydrides is removed as H₂ and the carboxylate anion takes its place, bridging the two metal centers.^{19,14} Three different carboxylic acids have been used for the synthesis of the dyes and, in particular, 4(diphenylamino)benzoic acid (TPA-COOH) for dye **1** and the carboxylic acid of the **D35** for dyes **2** and **3**.



Finally, substitution of the oxadiazole with properly functionalized diazine ligands, (namely the pyridazinyl-carboxylic acid for dyes **1** and **2** and the pyridazinyl-4-butyric acid for dye **3**, respectively) afforded the desired products.



Scheme 1: Synthetic pathways for the preparation of rhenium hydrido-carboxylato dyes 1-3.

Electrochemical characterization

Cyclic voltammetry analysis has been performed on all the derivatives **1-COOMe**, **2-COOMe** and **3-COOMe** containing the methyl ester of the corresponding diazine ligand, in order to avoid the reduction of the acidic proton, and H_2 evolution. The cyclic voltammetry behavior in acetonitrile, at 298 K, is reported in Figure 1 and the peak potentials, together with the related HOMO and LUMO energy values, are reported in Table 1. In the cathodic region dye **2**, containing the same diazine ligand of **1**, displays the same behavior previously reported: namely one monoelectronic reduction peak at about -0.9 V (vs. $\text{Fc}^+|\text{Fc}$), which is centered on the diazine ligand and whose chemical reversibility is confirmed by the presence of its anodic counterpart. On the contrary, for dye **3**, the reduction peak is observed at -1.47 V, i.e. at the same reduction potential of the complex $[\text{Re}_2(\mu\text{-Cl})_2(\text{CO})_6(\mu\text{-4-}n\text{-hexylpydz})]$ (-1.46 V)²⁰ containing a pyridazine ligand functionalized in one of the β position with a similar aliphatic chain. Also in this case, the reduction is chemically and electrochemically reversible. It is interesting to note that the peak potential is slightly modulated by the different nature of the ancillary ligand, in agreement with the different localization of the ground-state energy levels.

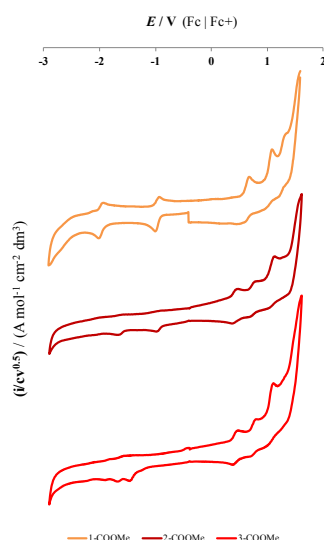
View Article Online
DOI: 10.1039/C9CP00856J

Figure 1: Normalized CV features of the methyl-ester derivatives of dyes **1-3** on GC electrodes, in ACN + 0.1 M TBAPF₆ solution, at 0.2 V s⁻¹ with ohmic drop compensation

All these features are in agreement with the localization of the reduction process on the diazine ring, as indicated also by the description of the LUMO provided by the DFT computations.^{17,20} Therefore, the LUMO level results stabilized, and partially delocalized, by the presence of the carboxylic group in β position, as in the dyes **1** and **2**. On the other hand, a partial destabilization of the LUMO is observed in presence of the electron-donor alkyl chain, as in the case of **3**.

In the anodic part, dyes **1-3** display a close sequence of three mono-electronic oxidation peaks. The two oxidation processes, observed at the highest potentials, are clearly localized on the metal core. This attribution is confirmed both by the computational analysis and by the comparison with the electrochemical behavior already observed in the derivatives containing alcoholate, phenolate²¹ and benzoate¹⁴ anions as ancillary ligands. Moreover, these oxidation potentials are lower for dyes **2** and **3** than for dye **1** (+0.75 V vs +1.07, see Table 1) and this is due to the presence of the strong electron-withdrawing acrylonitrile moiety, bound to the coordinating carboxylate group. These data still confirm that the oxidation process is markedly different in the case of the oxygen-bridged derivatives compared to the dichloride¹⁷ or chalcogenide ones,²² and probably related to the harder nature of the oxygen as donating atom in bridging ligands.

Beside the two oxidation peaks centered on the metal core, another chemically reversible oxidation peak at lower potential is observed (see Table 1 and Figure 1). This peak is clearly attributed to the formation of a radical cation on the triarylamine (TPA) moiety, as indicated either by the comparison with the electrochemical behavior of the free 4-diphenylamino-benzoic acid ($E_{p,a} = 0.70$ V)¹⁴ and by the modulation of the peak potential by the substituents on the TPA core. Indeed, dyes **2** and **3**, containing a more conjugated TPA moiety, display a lower oxidation potential than dye **1** (+0.66 V vs +0.41 V, see Table 1).

Table 1: First reduction and oxidation peak potentials ($E_{p,c}$ and $E_{p,a}$) and electrochemical (ΔE_e) and spectroscopic (ΔE_s)^a energy gaps of the dyes. Potentials are referred to the Fc⁺|Fc couple^b in the operating medium (ACN, 0.1 M TBAPF₆). Scan rate 0.2 V s⁻¹. ^aThe spectroscopic (ΔE_s) energy gap is the energy associated with the electronic transition determined from the maximum of the ¹MLCT absorption band. ^b Fc⁺|Fc potential is 0.385 V vs. SCE in ACN solution.

COMPLEX	$E_{p,c}$ [V]	$E_{p,a}$ [V]	ΔE_e [eV]	ΔE_s [eV]	E_{LUMO} [eV]	E_{HOMO} [eV]
1-COOMe	-0.97	0.66, 1.07, 1.32	1.64	2.56	-3.81	-5.45
2-COOMe	-0.94	0.41, 0.74, 1.10	1.36	2.52	-3.85	-5.21
3-COOMe	-1.42	0.42, 0.75, 1.10	1.84	2.55	-3.37	-5.21

Spectroscopic characterization

UV-Vis absorption maxima and molar absorptivities are reported in Table 2 both in solution and adsorbed on TiO₂, while Figure 2 shows all the spectra in toluene solution. In solution, all the dyes exhibit two broad and featureless absorption bands extending in a conspicuous part of the visible spectrum between 300 nm and 600 nm.

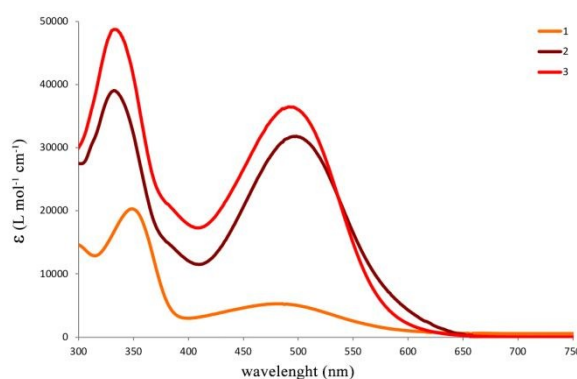


Figure 2: UV-Vis absorption spectra of dyes 1-3 in toluene solution.

The low energy absorption band is ascribable to the metal-to-ligand $d\pi(\text{Re}) \rightarrow \pi^*$ (diazine) charge transfer transition ($^1\text{MLCT}$), in agreement with the DFT computations and by comparison with the analogous complexes of this family.¹⁷ This broad MLCT band arises from the convolution of multiple transitions, as testified by the more or less pronounced shoulders observed at longer wavelengths. This attribution is supported either by their solvatochromic behavior, and by the presence of the predicted red-shift in the absorption maximum for the **D35**-based dyes **2** and **3**, compared to the bare TPA-based dye **1**. In addition, dyes **2** and **3** show an impressive tenfold increase in the value of the ϵ compared to **1**, therefore greatly improving the light harvesting. This is due to a partial superposition between the MLCT band and the absorption band of the **D35** ligand, which displays an absorption band at 500 nm in CH_2Cl_2 solution with a high molar extinction coefficient ($31300 \text{ M}^{-1}\text{cm}^{-1}$).¹⁶

Table 2: UV-Vis MLCT absorption data of the dyes in solution and on TiO_2 film. ^a toluene solution ($2 \times 10^{-5} \text{ M}$). ^b EtOH solution ($2 \times 10^{-5} \text{ M}$). ^c TiO_2 film. Absorption data for **D35**: $31300 \text{ M}^{-1}\text{cm}^{-1}$ at 500 nm.

COMPLEX	$\lambda_{\text{max}}^a / \text{nm}$	$\epsilon / \text{M}^{-1}\text{cm}^{-1}$	$\lambda_{\text{max}}^b / \text{nm}$	$\lambda_{\text{max}}^c / \text{nm}$
1	483	$5.2\text{E}+03$	425	443
2	493	$3.1\text{E}+04$	486	487
3	486	$3.5\text{E}+04$	487	493

All the dyes also display another higher energy absorption band around 335-350 nm, whose position is completely independent from the polarity of the solvent. In agreement with the electrochemical and computational data already reported for dye **1**,¹⁴ this band is attributed to the $\pi-\pi^*$ transition involving the triarylamine moiety. Noticeably, for dyes **2** and **3**, containing the more conjugated **D35** ligand, this band is moderately blue-shifted, as a consequence of the presence of two butoxyphenyl electron donating units on the TPA moiety of **D35**.

Devices

Photovoltaic measurements have been carried out to evaluate the potential of the new rhenium complexes as dyes in DSSC devices. The main photovoltaic parameter performances of the solar cells under AM 1.5 G at 1 Sun (1000 W m^{-2}) illumination are presented in Table 3 and the current–voltage ($J-V$) curves are reported in Figure 3.

Sets of cells have been prepared and measured, changing one parameter at a time, in order to find the best operating conditions for each of these parameters. Dye **1**, already tested in an optimized device¹⁴ has been also re-tested after the engineering of optimized cells. In particular, different semiconductor oxides (TiO_2 , SnO_2)²³ have been tried in single or stacked-layer architecture, along with their relative thickness. The dyes have been adsorbed on the semiconductors in different media to find out the best solvent and adsorption time. At the same time, various counter electrode glasses with different sheet resistance have been tested with our dyes. The nature of the electrolytes has been also intensively investigated and the behavior of each dyes has been tested in two different types of electrolyte; one based on the iodide/triiodide redox shuttle, the other employing $\text{Co}^{2+/3+}$ metal complexes. Each electrolyte has been coupled with a suitable counter electrode: platinum for iodine, carbon for cobalt. Both the electrolytes have been developed in-house, the first one was labeled IE, the latter one CE.

The composition of both iodine based and cobalt based electrolytes has been varied to obtain the best current-voltage compromise. We have used cells with pure **D35** as photosensitizers as reference for this comparison. Solid-state devices (SSD) have been also prepared to investigate if these dyes may hold potential for this kind of devices. However, the generally low efficiencies detected prevented us from carrying out further investigations.

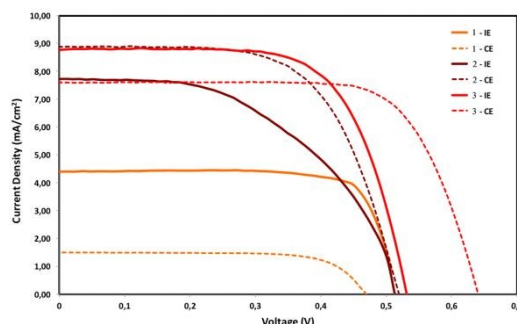


Figure 3: Current–voltage curves for optimized devices sensitized by renum-based dyes **1-3** under 1 Sun illumination, AM 1.5

The values related to the performances of the cells, reported in Table 3, clearly indicated that a careful engineering of the cells has afforded a new maximum performance of 1.8% for dye **1**, nearly doubling the previous value obtained for such dye.¹⁴

Table 3: Photovoltaic parameters for optimized and solid-state cells sensitized by **1-3** compared to **D35** using homemade Iodine based (IE) and cobalt (CE) electrolytes

CELL	$J_{sc}/\text{mA cm}^{-2}$	V_{oc}/V	FF	$\eta/\%$
1 IE/Pt	-4.5	0.51	78	1.8
1 CE/C	-1.4	0.47	72	0.5
1 SSD	-0.5	0.52	57	0.15
2 IE/Pt	-7.9	0.52	51	2.05
2 CE/C	-9.1	0.54	64	3.0
2 SSD	-0.4	0.46	53	0.35
3 IE/Pt	-8,8	0.54	67	3.15
3 CE/C	-7.6	0.65	71	3.5
3 SSD	-1.1	0.48	63	0.32
D35 CE/C	-11	0.88	72	7

A substantial increase in the photogenerated currents can be observed (see Table 3) for dyes **2** and **3** compared to dye **1**, due to the presence of the highly light-absorbing **D35** moiety. It is confirmed also by the incident photon-to-current conversion efficiency (IPCE) plots. Indeed, the monochromatic IPCE spectra, reported in Figure 4, show that the highest IPCE is obtained from the solar cell sensitized by **3** that, however, is not as red as **2**.

Due to the introduction of **D35**, the new dyes appear to work best in CE/C conditions, while dye **1**, with a simple triarylamine, remains more efficient in IE/Pt condition. The performances of dye **2** result only slightly better than those of **1** in IE conditions, affording 2%, while, in CE conditions, a value of 3% in efficiency can be reached. The best performing cells are sensitized by dye **3**, giving an overall power conversion efficiency of 3.15% (IE) and 3.5% (CE). The recombination between the electron in TiO_2 and the oxidized dye or between the electron in TiO_2 and the electrolyte, are crucial factors for the performances of the cells. The introduction of the **D35** moiety in dye **2** and **3** clearly contributes to further suppress the former recombination, thus improving the charge separation on TiO_2 . Moreover, the higher steric hindrance of **D35** also reduces the back reaction between the injected electron and the electrolyte. The recombination process with the oxidized dye is further suppressed in dye **3**, in which the presence of the less electron-withdrawing diazine affords a gain both in J_{sc} and V_{oc} , leading to a 3.5% efficiency. Indeed, by replacing the direct carboxylic moiety with the 4-butanoic acid derivative, the electron injection into the conduction band of TiO_2 got retarded, as proofed by Durrent, et al.²⁴, to minimize the kinetic redundancy. This adjustment prolongs the electron lifetime in the photoelectrode before recombining with the oxidized dye and/or cation in the electrolyte.

The external efficiency values, however, remain well under from those obtained under similar conditions by cells assembled using the conventional **D35** dye, reaching 7% (CE).

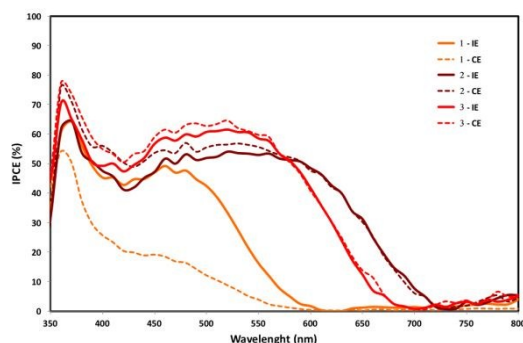


Figure 4: IPCE spectra for optimized devices sensitized by rhenium-based dyes 1-3.

Even though dye **2** and **3** have a similar or even wider light absorption compared to **D35**, this superior property does not reflect in the device efficiency. This is the case for dye **2** that has the smallest energy gap (see Table 1). Dye **2** can harvest the photons the most among the tested dyes. However, due to the several reasons (discussed below), dye **2** did not show the best properties, even for photocurrent. This can be explained by desorption of the dye and it is also confirmed by the electrochemical impedance spectroscopy (EIS).

From the analysis after electrochemical impedance spectroscopy, it was found that the charge transfer resistance at the counter electrode for dye **2** is higher than other samples (data not shown). It implies the desorption of dye **2** from the surface of TiO_2 and then, adsorption of them on the surface of counter electrode. Such phenomena can explain one of the reasons for the lower fill factor for the sample with dye **2**. Moreover, the desorption of dye molecules from the surface of TiO_2 causes the negative influence for the solar cell properties, such as drop on light harvesting and increase of the TiO_2 surface area which is exposed to the electrolyte.

The expected voltage shift from the conduction band movement due to the massive presence of Li^+ in the electrolyte is significant, once again, only for dye **2**. Moreover, the presence of Li^+ shifts down the conduction band of TiO_2 more for devices with Co as electrolyte than those with iodide. This feature affects also the open current voltage (V_{OC}) which is calculated by the difference between the Fermi level of the TiO_2 and the redox potential of the electrolyte. For the cells with Co redox couple, the V_{OC} increases on going from **1** to **3** and the difference with the V_{OC} of the cells with iodide, is smallest for complex **2**. This is in agreement with the desorption of dye **2** which leaves larger surface area exposed to the electrolyte allowing therefore the Li^+ to come at the surface of TiO_2 . The lowering of the conduction band of TiO_2 for the sample with dye **2** improves the electron lifetimes since the driving force between the conduction band of TiO_2 and the electrolyte is reduced, and so the transport efficiency, which are the best for dye **2**.

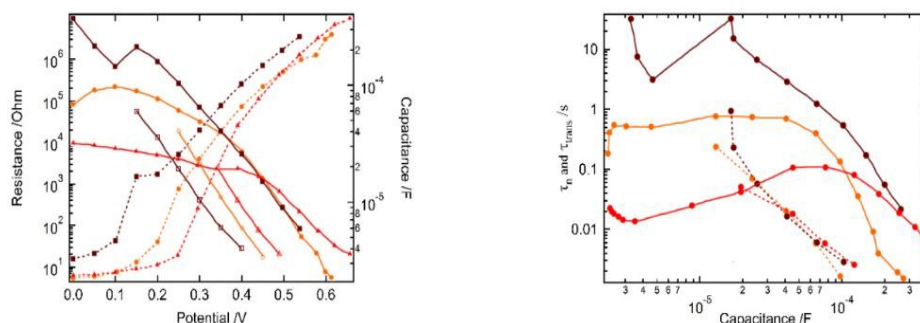


Figure 5: Left: resistance vs potential (solid curves: R_{ct} ; solid straight lines: R_{trans} ; dotted curves: C) and right: electron lifetimes vs capacitance (solid lines: lifetime; dotted lines: transport time) plots for devices sensitized by dyes **1** (orange line), **2** (brown line) and **3** (red line) in IE/Pt conditions.

In the case of the cobalt based electrolyte EIS shows a similar tendency (Figure 6). The conduction band of **2** is once again the lowest among all the complexes, while **3** owns a slightly higher one compared to **1**, as expected after the introduction of a non-conjugated

chain. The lifetimes are, in the case of the cobalt electrolytes, relatively similar between the three different dyes, but also in this case complex **2** shows the longest one.

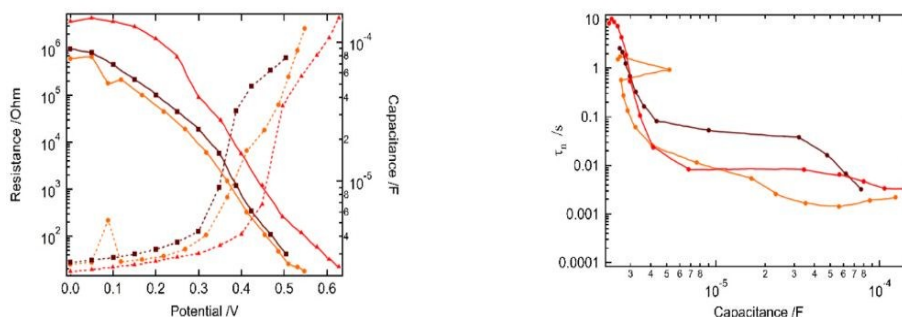


Figure 6: Left: resistance vs potential (solid line: R_{ct}; dotted line: C) and right: electron lifetimes vs capacitance plots for devices sensitized by dyes **1** (orange line), **2** (brown line) and **3** (red line) in CE/C conditions.

Conclusions

In our previous work, quantummechanical calculations using density functional theory (DFT) and time-dependent density functional theory (TDDFT) have been coupled with UV/vis absorption spectroscopy and preliminary photovoltaic device testing. Based on these results, we have here designed and synthesized new Dirhenium complex dyes. We have analyzed their electronic/optical properties and characterized the nature of their interaction with the TiO₂ substrate. Dye-sensitized solar cells were prepared and tested in operating solar cells. Light to-current conversion has been observed for all the investigated dyes with a significant improvement in terms of photocurrent and efficiency to respect the previously reported data. These interesting results are mainly due to the introduction of the triarylamine-based **D35** as carboxylate ligand, that further suppresses the recombination of the injected electron with the oxidized state of the dye. This wider light-harvesting and bulkier triarylamine moiety also reduces the back-reaction of the injected electron with the electrolyte. The best results have been obtained for the hydrido-carboxylato dye **3**, with a power conversion efficiency of 3.5 %. This feature resulted by combining molecular design for a higher LUMO and a better anchoring to TiO₂ surface, with optimization of the cell device after characterizing the other two dyes, **1** and **2**, which performed less represented by the excessive stabilization of the π* orbitals of the diazine and by the desorption of the dye. In summary, the presence of the bulkier triphenylamine moiety and the use of an electron-rich ligand successfully improved the photovoltaic efficiency, due to the reduced recombination and an optimization of the kinetic retardation. However, there are still challenges, such as dye-aggregation, further tuning of HOMO-LUMO energy level for realizing high efficiency dye-sensitized solar cells.

As the last notable point, the three-step synthetic procedure here developed has a wider scope than the preparation of the compounds here described and opens the way to a large number of dinuclear complexes of this family, tailored to specific applications.

Experimental

Materials and Methods

All the reactions are performed under a nitrogen atmosphere unless specified otherwise. The reagents are purchased from Aldrich, Fluka and Lancaster and used as received. **D35** is purchased by Dyenamo and washed with H₂O then dried under vacuum before use. All the solvents are deoxygenated and dried by standard methods before use, toluene is distilled on Na(s) and CH₂Cl₂ on P₂O₅, both under N₂ atmosphere. Commercial deuterated solvents are used as received. Column chromatography is performed using Alfa Aesar silica gel 60 (0.032–0.063 mm). [Re₄(μ₃-H)₄(CO)₁₂](C₆H₆)₂,²⁵ [Re₂(μ-H)₂(CO)₆(μ-ppd)] (ppd = 2,5-diphenyl-1,3,4-oxadiazole)¹⁸ and

$[\text{Re}_2(\mu\text{-H})(\mu\text{-4-OOC-TPA})(\text{CO})_6(\mu\text{-pydz-4-COOH})]$ (**1**) (4-OOC-TPA = 4-(diphenylamino)benzoate anion pydz-4-COOH = pyridazine-4-carboxylic acid)¹⁴ are synthesized according to literature procedures. IR spectra in solution are acquired on a Bruker Vector 22 FT spectrophotometer. Solution and thin-film UV/Vis absorption spectra are obtained using an Agilent 8453 spectrophotometer, fused quartz cuvettes (10 mm optical path), and CHROMASOL V grade solvents. IR spectra are acquired on a Bruker Vector 22 FT spectrophotometer.

Synthesis

Synthesis of $[\text{Re}_2(\mu\text{-H})(\mu\text{-D35})(\text{CO})_6(\mu\text{-ppd})]$. 40 mg (0.046 mmol) of solid **D35** are added to a solution of 32 mg (0.042 mmol) of $[\text{Re}_2(\mu\text{-H})_2(\text{CO})_6(\mu\text{-ppd})]$ previously dissolved in 5 mL of anhydrous toluene. The reaction mixture is left stirring under reflux overnight, then the solution evaporated to dryness under vacuum. The obtained solid is purified through column chromatography (eluent $\text{CH}_2\text{Cl}_2/\text{Hexane}$ 75:25), then dried under vacuum, yielding 30 mg (0.018 mmol) of brick-red powder (yield 44%). IR (CH_2Cl_2) $\nu(\text{CO})$: 2042 (s), 2024 (vs), 1937 (vs), 1917 (s) cm^{-1} . ^1H NMR: (CD_2Cl_2 , 300K, 400 MHz) δ_{H} (ppm) 8.18 (d, $J = 7.5$ Hz, 4H, Hortho ppd), 7.90 (m, 2H, Hpara ppd), 7.79 (m, 4H, Hmeta ppd), 8.16 (s, 1H), 7.75 (d, $J = 4.2$ Hz, 1H), 7.60 (d, $J = 8.88$ Hz, 2H), 7.52 (d, $J = 8.47$ Hz, 4H), 7.37 (d, $J = 4.2$ Hz, 2H), 7.29 (d, $J = 9.3$ Hz, 2H), 7.21 (d, $J = 8.47$ Hz, 4H), 7.17 (d, $J = 8.88$ Hz, 2H), 6.59 (s, 2H), 6.58 (m, 2H), 4.02 (t, $J = 6.98$ Hz, 4H, CH₂), 4.01 (t, $J = 6.98$ Hz, 4H, CH₂), 1.79 (m, 8H, CH₂), 1.57 (m, 4H, CH₂), 1.50 (m, 4H, CH₂), 1.03 (m, 6H, CH₃), 0.97 (m, 6H, CH₃), -7.14 (s, 1H, hydride). Elemental anal. calcd. for $\text{C}_{74}\text{H}_{68}\text{N}_4\text{O}_{12}\text{SRe}_2$: C, 54.67; H, 4.22; N, 3.45. Found: C 55.31, H 4.83, N 3.27.

Synthesis of $[\text{Re}_2(\mu\text{-H})(\mu\text{-D35})(\text{CO})_6(\mu\text{-pydz-4-COOH})]$ (2**).** Once 15 mg (0.009 mmol) of $[\text{Re}_2(\mu\text{-H})(\mu\text{-D35})(\text{CO})_6(\mu\text{-ppd})]$ are dissolved in 5 mL of freshly distilled and degassed THF, 1.5 mg (0.01 mmol) of 4-pyridazine-carboxylic acid are added to the reaction mixture. The reaction is set at 85°C for 2 hours. The solution is evaporated to dryness under vacuum, the crude product dissolved in CH_2Cl_2 and re-precipitated with n-hexane. The supernatant solution is removed and the remaining powder is washed with hexane (3 mL) five times, and dried under vacuum affording 11 mg (0.072 mmol) of the desired product (yield 80%). IR (CH_2Cl_2) $\nu(\text{CO})$: 2040 (m), 2020 (s), 1938 (s), 1920 (m) cm^{-1} . ^1H NMR: (CD_2Cl_2 , 300K, 400 MHz) δ_{H} (ppm) 9.75 (s, 1H, H₃ pydz-4-COOH), 9.51 (d, $J = 5.6$ Hz, 1H, H₆ pydz-4-COOH), 8.39 (dd, $J = 4.7, 2.9$ Hz, 1H, H₅ pydz-4-COOH), 8.13 (s, 1H), 7.73 (m, 1H), 7.62 (m, 2H), 7.51 (m, 4H), 7.36 (m, 2H), 7.27 (m, 2H), 7.22 (m, 4H), 7.18 (m, 2H), 6.59 (s, 2H), 6.57 (m, 2H), 4.02 (t, $J = 6.98$ Hz, 4H, CH₂), 4.01 (t, $J = 6.98$ Hz, 4H, CH₂), 1.79 (m, 8H, CH₂), 1.53 (m, 4H, CH₂), 1.49 (m, 4H, CH₂), 1.03 (t, $J = 7.4$ Hz, 6H, CH₃), 0.97 (t, $J = 7.4$ Hz, 6H, CH₃), -6.75 (s, 1H, hydride). Elemental anal. calcd. for $\text{C}_{65}\text{H}_{62}\text{N}_4\text{O}_{14}\text{SRe}_2$: C, 51.10; H, 4.09; N, 3.67. Found: C 52.09, H 4.42, N 3.19.

Synthesis of $[\text{Re}_2(\mu\text{-H})(\mu\text{-D35})(\text{CO})_6(\mu\text{-4-pyridazinyl-butanoic acid})]$ (3**).** 15 mg (0.009 mmol) of $[\text{Re}_2(\mu\text{-H})(\mu\text{-D35})(\text{CO})_6(\mu\text{-ppd})]$ are dissolved in 5 cm^3 of freshly distilled and degassed THF, 2 mg (0.012 mmol) of 4-pyridazinyl-butanoic acid are added to the reaction mixture. The reaction is put under reflux for 2 hours. The solution is evaporated to dryness under vacuum, the crude product dissolved in CH_2Cl_2 , and re-precipitated with n-hexane. The supernatant solution is removed and the remaining powder is washed with hexane (3 cm^3) five times, then dried under vacuum affording 11 mg (0.007 mmol) of red powder (yield 78%). IR (CH_2Cl_2) $\nu(\text{CO})$: 2042 (m), 2024 (s), 1943 (s), 1921 (m) cm^{-1} . ^1H NMR: (CD_2Cl_2 , 300K, 400 MHz) δ_{H} (ppm) 9.22 (d, $J = 5.9$ Hz, 2H, H₆ 4-pydz-BuCOOH), 9.21 (d, $J = 5.9$ Hz, 2H, H₃ 4-pydz-BuCOOH), 8.12 (s, 1H), 7.78 (d, $J = 2.0$ Hz, 1H, H₅ 4-pydz-BuCOOH), 7.74 (d, $J = 4.1$ Hz, 1H), 7.60 (d, $J = 8.88$ Hz, 2H), 7.52 (d, $J = 8.6$ Hz, 4H), 7.36 (d, $J = 4.1$ Hz, 2H), 7.28 (m, 2H), 7.21 (d, $J = 8.8$ Hz, 4H), 7.17 (d, $J = 7.4$ Hz, 2H), 6.59 (s, 2H), 6.58 (d, $J = 6.8$ Hz, 2H), 4.02 (t, $J = 6.98$ Hz, 4H, CH₂), 4.01 (t, $J = 6.98$ Hz, 4H, CH₂), 1.79 (m, 8H, CH₂), 1.56 (m, 4H, CH₂), 1.47 (m, 4H, CH₂), 1.03 (m, 6H, CH₃), 0.97 (m, 6H, CH₃), -6.65 (s, 1H, hydride). Elemental anal. calcd. for $\text{C}_{68}\text{H}_{68}\text{N}_4\text{O}_{14}\text{SRe}_2$: C, 52.02; H, 4.37; N, 3.57. Found: C 53.64, H 4.95, N 3.10.

Synthesis of methyl ester of pydz-4-COOMe and complexes (1-3)-COOMe. A sample of pyridazine-4-carboxylic acid (100 mg, 0.805 mmol) (for 1 and 2) or pyridazine-4-butanoic acid (134 mg, 0.805 mmol) for 3) was dissolved in MeOH (2 mL) and was treated with H_2SO_4 (40 mL, 96% w/w) at room temperature. The reaction mixture was heated at reflux temperature and was stirred overnight. Then, the solution was cooled at room temperature and the reaction was quenched by the addition of saturated solution of Na_2CO_3 until pH 8. The product was extracted with Et_2O and the organic fractions were collected, washed with brine, dried with Na_2SO_4 and

evaporated to dryness to leave a pale yellow solid (isolated yield 30%). $^1\text{H NMR}$ (DMSO, 300 K, 400 MHz) δH (ppm) 9.58 (s, 1H, H_{ortho}), 9.51 (d, 1H, H_{ortho}), 8.09 (dd, 1H, H_{meta}), 3.94 (s, 3H, CH_3). This pyridazine was used to synthesize the corresponding derivatives **1-COOMe**, **2-COOMe** and **3-COOMe** according to the previous procedures.

Electrochemical measurements The cyclic voltammetric study of the complexes has been performed at scan rates typically ranging from 0.02 to 10 V s^{-1} in HPLC-grade acetonitrile (MeCN) solutions at 2.5×10^{-4} M concentration in each substrate, deaerated by N_2 bubbling with 0.1 M TBAPF₆ (TBA = NBu_4 , Aldrich) as the supporting electrolyte, at 298 K. The ohmic drop has been compensated by the positive feedback technique. The experiments were carried out using an AUTOLAB PGSTAT potentiostat (EcoChemie, The Netherlands) run by a PC with GPES software. The working electrode was a glassy carbon one (AMEL, diameter 1.5 mm) cleaned by diamond powder (Aldrich, diameter 1 mm) on a wet cloth (STRUERS DP-NAP); the counter electrode was a platinum wire; the reference electrode was an aqueous saturated calomel electrode, having in our working medium a difference of 0.385 V vs. the Fc^+/Fc couple (the intersolvent redox potential reference currently recommended by IUPAC).

DSSC and SSD preparation The solution-processed and the solid-state devices were made using respectively, 18 NR-T and 30 NR-D titanium oxide (TiO_2) paste obtained from Dyesol. Lithium iodide (LiI), lithium bis(trifluoromethane)sulfonimide (LiTFSI), iodine, tert-butyl pyridine (TBP), and guanidinium thiocyanate (GuSCN) were purchased from Aldrich, and 2,2',7,7'-tetrakis-(N,N-di-4-methoxyphenylamino)-9,9'-spirobifluorene (Spiro-OMeTAD) was obtained from Solaronix. $[\text{Co}(\text{bpy})_3(\text{B}(\text{CN})_4)_2]$ and $[\text{Co}(\text{bpy})_3(\text{B}(\text{CN})_4)_3]$ were synthesized at EPFL. The homemade substrates for liquid-containing cells have a size of approximately 1.4 cm \times 1.6 cm, with an active area of 0.159 cm^2 . The device structure consists of a transparent fluorine doped tin oxide (FTO) layer as the bottom electrode, supported on a NSG TEC C10 glass substrate. After being cleaned and having undergone UV- O_3 treatment for 15 minutes, the FTO glass plates were immersed in a 40 mM aqueous TiCl_4 solution at 70 $^\circ\text{C}$ for 35 min and then washed with water and ethanol. Two screen-printed layer of nanocrystalline TiO_2 particles were used as the photoelectrode. The transparent mesoporous layer (tl), made of 18 nm sized TiO_2 particles (Dyesol DSL18NR-T) was printed on the FTO conducting glass, and the plates were then heated at 150 $^\circ\text{C}$ for 7 min. To render high PCE, a ~ 5 - μm scattering layer (sl, 400 nm diameter, Catalysts & Chemicals Ind. Co. Ltd. (CCIC), HPW-400) was deposited on the transparent layer. A total film thickness of 7(tl) + 5(sl) μm was used. Sintering was carried out following a 4-step temperature ramp from 175 to 500 $^\circ\text{C}$, with a residence time of 30 min. The sintered glass plates were immersed again in a 20 mM aqueous TiCl_4 solution at 70 $^\circ\text{C}$ for 35 min and washed with water and ethanol. The films were heated again at 500 $^\circ\text{C}$ for 30 min using a heat blower followed by cooling to 90 $^\circ\text{C}$ and dipping into a 0.3 mM toluene solution of the dyes overnight at room temperature. To prepare the counter-electrode, Pt catalyst was deposited on cleaned TEC 15 FTO glass by coating with a drop of H_2PtCl_6 solution (5 mM in 2-PrOH solution) with subsequent rapid thermal treatment at 400 $^\circ\text{C}$ for 15 min. Carbon counter-electrodes followed the same procedure with a graphite/acetone solution. For the assembly of DSSCs containing liquid electrolyte, the dye-containing TiO_2 electrode and the counter-electrode were assembled into a sandwich-type cell and sealed with a hot-melt gasket of 25 μm thickness made of the ionomer Surlyn 1702 (Dupont). The redox electrolyte was driven into cells through two holes previously drilled in the counter-electrode. The iodine-based type of electrolyte used for rhenium-based dyes, consists of 0.7 M LiI, 0.025 M I₂ and 0.2 M TBP in ACN. The cobalt-based type of electrolyte contained instead 1 M LiTFSI, 0.33 M $[\text{Co}(\text{bpy})_3(\text{B}(\text{CN})_4)_2]$, 0.06 M $[\text{Co}(\text{bpy})_3(\text{B}(\text{CN})_4)_3]$ and 0.2 M TBP in ACN. Finally, the hole was sealed using Surlyn and a cover glass (0.1 mm thickness). Solid state devices (SSD) were prepared following a similar procedure. An FTO glass plate of 1.4 cm \times 2.3 cm was laser etched to create non-conductive zone for separation of the contacts, then was cleaned and UV/ O_3 treated before undergoing flame spray pyrolysis. A solution containing 0.6 mL of titanium isopropoxide acetylacetonate $[\text{Ti}(\text{OiPr})_2(\text{acac})_2]$, 0.4 mL of acetylacetonone and 9 mL of ethanol was then sprayed (gas carrier: O_2 , 0.8 bar) on the glass plates at 450 $^\circ\text{C}$, creating a non-porous transparent TiO_2 layer. The transparent mesoporous layer, in this case made of 30 nm sized TiO_2 particles (Dyesol DSL30NR-D) was printed with a different mesh on the FTO conducting glass, followed by no scattering layer. Sintering was carried out as described above. The titania films were then dipped into a 0.3 mM toluene solution of the dyes overnight at room temperature, then dried, and transferred into a glove box. A solution of the hole transporting material (HTM), Spiro-OMeTAD, was spin coated onto the adsorbed dye. The final thickness of the whole cell

resulted to be around 2 μm . The counter-electrode, metallic gold, was deposited via physical vapor deposition, without sealing the cell before measurements. DOI: 10.1039/C9CP00856J

DSSC and SSD characterization All measurements were carried out in air directly after the fabrication of the cells. A black shadow mask with a fixed aperture was used on DSSCs and SSDs, so that the active area was set to 0.16 cm^2 . Current-voltage characteristics were recorded by applying an external potential bias to the cell while recording the generated photocurrent with a digital source meter (Keithley model 2400) connected to a pc. The light source was a 450 W xenon lamp (Oriol) equipped with a Schott K113 Tempax sunlight filter (Präzisions Glas & Optik GmbH) to match the emission spectrum of the lamp with the AM 1.5 G standard. Before each measurement, the exact light intensity was determined using a calibrated Si reference diode equipped with an infrared cutoff filter (Schott KG-3). The incident photon to collected electron conversion efficiency (IPCE) measurement was plotted as function of wavelength by using the light from a 300-W xenon lamp (ILC Technology), which was focused through a Gemini-180 double monochromator (Jobin Yvon) onto the photovoltaic cell under test. A computer-controlled monochromator was incremented through the spectral range (300–800 nm) to generate a photocurrent action spectrum with a sampling interval of 10 nm and a current sampling time of 4 s to reduce scattered light from the edge of the glass electrodes of the dyed TiO_2 layer. Electrochemical impedance spectroscopy (10 mV steps in the 10⁻¹-10⁻⁶Hz range) has been carried out only on transparent layer-only version of the already assembled DSSC cells, using a BioLogic SP-300 potentiostat with Zview software, at open circuit, both in the dark and under illumination. Spectra were analyzed with Zview equivalent circuit modeling software, including the distributed element DX11 (transmission line model). All the measurements were performed one day after cell preparation.

Conflicts of interest

There are no conflicts to declare.

Acknowledgements

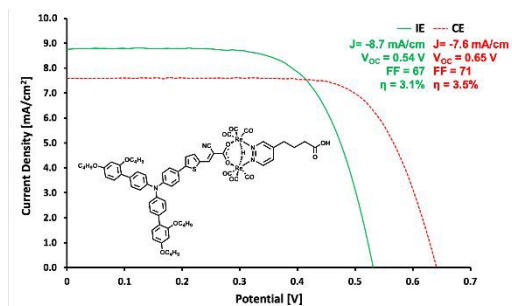
The use of instrumentation purchased through the Regione Lombardia – Fondazione Cariplo joint SmartMatLab Project (2013-1766) is gratefully acknowledged.

Notes and references

1. B. O'Regan, M. Grätzel, *Nature* 1991, **353**, 737.
2. T. M. Brown, F. De Rossi, F. Di Giacomo, G. Mincuzzi, V. Zardetto, A. Reale, A. Di Carlo, *J. Mater. Chem. A*, 2014, **2**, 10788.
3. A. Fakharuddin, R. Jose, T. M. Brown, F. Fabregat-Santiago, J. Bisquert, *Energy Environ. Sci.*, 2014, **7**, 3952.
4. M. Nazeeruddin, F. De Angelis, S. Fantacci, A. Selloni, G. Viscardi, P. Liska, S. Ito, B. Takeru, M. Grätzel, *J. Am. Chem. Soc.*, 2005, **127**, 16835–16847.
5. D. Kuang, S. Ito, B. Wenger, C. Klein, J. Moser, R. Humphry-Baker, S. Zakeeruddin, M. Grätzel, *J. Am. Chem. Soc.*, 2006, **128**, 4146–4154.
6. S. Mathew, A. Yella, P. Gao, R. Humphry-Baker, B.F. E. Curchod, N. Ashari-Astani, I. Tavernelli, U. Rothlisberger, Md. K. Nazeeruddin, M. Grätzel, *Nature chemistry* 2014, **6**, 242-247.
7. (a) M. Nazeeruddin, A. Kay, I. Rodicio, R. Humphry-Baker, E. Müller, P. Liska, N. Vlachopoulos, M. Grätzel, *J. Am. Chem. Soc.*, 1993, **115**, 6382–6390; (b) K. Kalyanasundaram, M. Grätzel, *Coord. Chem. Rev.*, 1998, **177**, 347–414.
8. S. Campagna, F. Puntoriero, F. Nastasi, G. Bergamini, V. Balzani, *Top Curr. Chem.* 2007, **280**, 117-214.
9. (a) S. Ferrere and B. A. Gregg, *J. Am. Chem. Soc.*, 1998, **120**, 843-844; (b) P. Balraju, M. Kumar, M. S. Roy and G. D. Sharma, *Synth. Met.*, 2009, **159**, 1325–1331.
10. T. Bessho, E. C. Constable, M. Grätzel, A. H. Redondo, C. E. Housecroft, W. Kylberg, M. K. Nazeeruddin, M. Neuburger and S. Schaffner, *Chem. Commun.*, 2008, 3717–3719; (b) C. L. Linfoot, P. Richardson, T. E. Hewat, O. Moudam, M. M. Forde, A. Collins, F. White and N. Robertson, *Dalton Trans.* 2010, **39**, 8945–8956.

11. (a) W. Wu, X. Xu, H. Yang, J. Hua, X. Zhang, L. Zhang, Y. Longa, H. Tian, *J. Mater. Chem.* 2011, **21**, 10666–10671; (b) E. A. M. Geary, L. J. Yellowlees, L. A. Jack, I. D. H. Oswald, S. Parsons, N. Hirata, J. R. Durrant and N. Robertson, *Inorg. Chem.*, 2005, **44**, 242–250.
12. B. Bozic-Weber, E. C. Constable, C. E. Housecroft, *Coord. Chem. Rev.* 2013, **257**, 3089–3106
13. (a) J. B. Asbury, E. Hao, Y. Wang, T. Lian, *J. Phys. Chem. B* 2000, **104**, 11957–11964; (b) N. A. Anderson, X. Ai, D. Chen, D. L. Mohler, T. Lian, *J. Phys. Chem. B* 2003, **107**, 14231–14239.
14. L. Veronese, E. Quartapelle Procopio, F. De Rossi, T. M. Brown, P. Mercandelli, P. Mussini, G. D'Alfonso, M. Panigati, *NewJ. Chem.*, 2016, **40**, 2910.
15. S. M. Feldt, E. A. Gibson, E. Gabrielsson, L. Sun, G. Boschloo, A. Hagfeldt, *J. Am. Chem. Soc.* 2010, **132**, 16714–16724.
16. X. Jiang, K. M. Karlsson, E. Gabrielsson, E. M. J. Johansson, M. Quintana, M. Karlsson, L. Sun, G. Boschloo, A. Hagfeldt, *Adv. Funct. Mater.* 2011, **21**, 2944–2952.
17. M. Panigati, M. Mauro, D. Donghi, P. Mercandelli, P. Mussini, L. De Cola, G. D'Alfonso, *Coord. Chem. Rev.*, 2012, **256**, 1621–1643.
18. M. Mauro, M. Panigati, D. Donghi, P. Mercandelli, P. Mussini, A. Sironi and G. D'Alfonso, *Inorg. Chem.*, 2008, **47**, 11154–11165.
19. E. Quartapelle Procopio, V. Bonometti, M. Panigati, P. Mercandelli, P. Mussini, T. Benincori, G. D'Alfonso and F. Sannicolo, *Inorg. Chem.*, 2014, **53**, 11242–11251.
20. The reduction potential is -1.34 V for the parent complex $[\text{Re}_2(\mu\text{-Cl})_2(\text{CO})_6(\mu\text{-pyridazine})]$ and -1.58 V for $[\text{Re}_2(\mu\text{-Cl})_2(\text{CO})(\mu\text{-4,5-Mez-pyridazine})]$ containing an electron-rich pyridazine ligand. See for instance M. Mauro, E. Quartapelle Procopio, Y. Sun, C.-H. Chien, D. Donghi, M. Panigati, P. Mercandelli, P. Mussini, G. D'Alfonso and L. De Cola, *Adv. Funct. Mater.*, 2009, **19**, 2607–2614.
21. A. Raimondi, M. Panigati, D. Maggioni, L. D'Alfonso, P. Mercandelli, P. Mussini, G. D'Alfonso, *Inorg. Chem.*, 2012, **51**, 2966–2975
22. L. Veronese, E. Quartapelle Procopio, D. Maggioni, P. Mercandelli, M. Panigati, *NewJ. Chem.*, 2017, **41**, 11268.
23. the data of devices with SnO_2 are reported in the supporting Information only for the dye **1**
24. J. E. Kroeze, N. Hirata, S. Koops, Md. K. Nazeeruddin, L. Schmidt-Mende, M. Grätzel, J. R. Durrant, *J. Am. Chem. Soc.* 2006, **128**, 16376–16383.
25. (a) M. A Andrews, S. W. Kirtley and H. D. Kaesz, *Inorg. Chem.*, 1977, **16**, 1556–1561; (b) J. R. Johnson and H. D. Kaesz, *Inorg. Synth.*, 1978, **18**, 60–62.

Table of Contents Entry

View Article Online
DOI: 10.1039/C9CP00856J

Dinuclear hydrido-carbonyl rhenium complexes first time for DSSCs. Molecular designing achieved an improved performance in solar cell efficiency.